

A likely inverse-Compton emission from the Type IIb SN 2013df

K. L. Li^{1,2,*} and A. K. H. Kong^{1,*}

¹Institute of Astronomy and Department of Physics, National Tsing Hua University, Hsinchu 30013, Taiwan

²Department of Physics and Astronomy, Michigan State University, East Lansing, MI 48824-2320, USA

*liliray@pa.msu.edu (KLL) and akong@phys.nthu.edu.tw (AKHK)

ABSTRACT

The inverse-Compton X-ray emission model for supernovae has been well established to explain the X-ray properties of many supernovae for over 30 years. However, no observational case has yet been found to connect the X-rays with the optical lights as they should be. Here, we report the discovery of a hard X-ray source that is associated with a Type II-b supernova. Simultaneous emission enhancements have been found in both the X-ray and optical light curves twenty days after the supernova explosion. While the enhanced X-rays are likely dominated by inverse-Compton scatterings of the supernova's lights from the Type II-b secondary peak, we propose a scenario of a high-speed supernova ejecta colliding with a low-density pre-supernova stellar wind that produces an optically thin and high-temperature electron gas for the Comptonization. The inferred stellar wind mass-loss rate is consistent with that of the supernova progenitor candidate as a yellow supergiant detected by the *Hubble Space Telescope*, providing an independent proof for the progenitor. This is also new evidence of the inverse-Compton emission during the early phase of a supernova.

Introduction

Supernova (SN) explosions produce strong X-ray emissions by the interactions between the fast outward-moving ejecta materials and the almost stationary circumstellar medium (CSM) deposited by the progenitors' stellar wind. The CSM would be heated up to $T \geq 10^9$ K by the forward shock (often termed as circumstellar shock) in which free-free cooling and/or inverse-Compton (IC) cooling are crucial to radiate the thermal energy out in X-rays within the first months^{1,2}. For electron temperatures of the shocked CSM, $T_e \geq 3 \times 10^9$, the effect of Comptonization on the X-ray emission becomes more important leading a domination over the free-free emission in 1–10 keV, even for a Compton-thin electron gas (i.e., $\tau_e \ll 1$)^{1,2}. As the luminosity and the spectral slope of the Comptonized flux strongly depends on the optical depth that is totally determined by properties of the pre-supernova stellar wind, observing the post-supernova X-rays provides a unique way to trace the mass-loss history of the SN progenitor that gives constraint on the fundamental stellar properties.

Supernova (SN) 2013df, residing in the constellation Coma Berenices, was discovered by the Italian Supernovae Search Project (ISSP) on 7.87 June 2013 UT with an apparent magnitude of 14th. Optical spectrum from the 10-meter Keck II telescope at Keck Observatory showed that it is a Type IIb SN with weak hydrogen emission features observed in the early phase³. The host galaxy of SN 2013df, NGC 4414, was observed on 1999 April 29 by the *Hubble* Heritage Project (GO/DD 8400; PI: Keith Noll) with the Wide Field and Planetary Camera 2 (WFPC2) of the *Hubble Space Telescope* (HST) of which a three-band (F439W, F555W, and F814W) image mosaic was obtained in total fourteen WFPC2 pointings with a total exposure time of 5400 sec. By matching the WFPC2 images with a post-explosion 20 sec exposure taken by HST/WFC3 (F555W) on 2013 July 15, a yellow progenitor candidate within an astrometric accuracy of 5.5 mas was discovered⁴. Although the source was undetected in WFPC2/F439W band with a 3σ lower limit of 25.65 mag, they concluded that the candidate progenitor is likely a yellow supergiant with an effective temperature of $T_{\text{eff}} = 4250 \pm 100$ K, a bolometric luminosity of $L_{\text{bol}} = 10^{4.94 \pm 0.06} L_{\odot}$, and an effective radius of $R_{\text{eff}} = 545 \pm 65 R_{\odot}$ by the absolute magnitudes of $V = -6.89$ mag and $I = -8.17$ mag. The authors also compared the maximum luminosity at the Type IIb secondary peak to those of the SNe IIb 1993J, 2008ax, and 2011dh and estimated less than $0.06 M_{\odot}$ of ^{56}Ni synthesized in the SN 2013df explosion.

In addition to the discovery of the yellow supergiant progenitor, another interesting scientific finding for SN 2013df is the early X-ray detection by the *Swift* X-ray Telescope (XRT)⁵. In spite of the limited resolution of *Swift*/XRT and the contamination from the diffuse emission of the host galaxy NGC 4414, the source is spectrally hard making it outstanding from the soft X-ray diffuse gas and showing the detection significance. Besides, early radio emissions were also detected by *electronic Multi-Element Radio Linked Interferometer Network* (eMERLIN; at 5 GHz⁶) and the *Very Large Array* (VLA; at various frequencies from 1.5 to 43.7 GHz⁷). While it has been suggested that the radio and X-ray emissions primarily originated from synchrotron and bremsstrahlung, respectively, we here present the X-ray spectrum and the multi-wavelengths light curve of SN 2013df and argue the origins of the X-rays to be dominated by the Compton scattering at the peak and the free-free emission in the rest of the time. In this work, the distance to NGC 4414 is assumed to be 16.6 Mpc⁸.

Results

X-ray/Optical Light curves

Double-peaked optical light curves are the most distinguished observational feature of Type IIb SNe. Shock wave heating of the progenitor's hydrogen envelope is the main cause of the first optical peak. While the amount of the hydrogen envelope (i.e., a few of $0.1 M_{\odot}$ ⁹) is insufficient to support a sustainable thermal radiation, the decay of ^{56}Ni synthesized in the explosion dominates the optical spectrum as the shock emission goes down, and produces the secondary optical peak¹⁰. In the case of SN 2013df, the secondary optical peak showed up at about day 20 since the SN discovery¹¹. Surprisingly, a simultaneous X-ray brightening ($\sim 4\sigma$ significance; see Methods for details) is also detected by *Swift*/XRT (Figure 1) with a photon index of $\Gamma = 1.7^{+1.2}_{-1.0}$ and an X-ray luminosity of $L_{1-7\text{keV}} \approx 3.2 \times 10^{39} \text{ erg s}^{-1}$ (1–7 keV; see Methods for details). From the *Swift*/UVOT v -band and X-ray light curves, the X-ray brightening reached the maximum as the secondary optical emission peaked. In addition to the synchronicity of the emission peaks, the rising and decaying rate of the X-ray flux is about the same as those of the optical lights. It is presumably more than a coincidence and the X-ray emission should be closely related with the SN photospheric radiation. This is reminiscent of Inverse-*Compton* scatterings of the SN lights by the shocked hot electron gas surrounding the SN as the source of the excess X-rays.

IC scattering as the origin of the X-ray peak

As mentioned in the introduction, IC is an important cooling process in the early phase of a SN, even if the shocked CSM electron gas (i.e., $T_e \geq 10^9 \text{ K}$) is *Compton*-thin (i.e., $\tau_e \sim 0.01$; see Methods for a detailed explanation). In fact, the IC X-ray spectrum can be described by a single power-law¹ and the spectral properties are closely related to the stellar wind (or the CSM) density of the progenitor, which can be represented by the ratio of the mass-loss rate (i.e., \dot{M}_{-5} in units of $10^{-5} M_{\odot} \text{ yr}^{-1}$) to the velocity (i.e., w_{10} in units of 10 km s^{-1}) of the pre-explosion wind. With the X-ray luminosity and the photon index obtained by *Swift*/XRT, we apply the inverse-*Compton* scattering model for SNe^{1,2,12} to explain the peak X-ray emissions observed in SN 2013df and constrain the wind parameters of the progenitor in the following (see Methods for a detailed description).

As the photons of the secondary SN peak are the seeds of the IC X-rays, the temperature and bolometric luminosity of the SN are both important to affect the IC emission. Adopting the blackbody temperature of the secondary peak of $T_c \approx 6900 \text{ K}$ ¹¹ and the absolute v -band magnitude of $M_v = -16.80 \text{ mag}$ ($D = 16.6 \text{ Mpc}$; see the Methods section), we estimated the bolometric luminosity, hence the radius of the SN photosphere, which is about $R_p \approx 1.4 \times 10^{15} \text{ cm} \approx 2.1 \times 10^4 R_{\odot}$. With an assumption of a typical SN shock velocity $V_s = 10^4 \text{ km s}^{-1}$ (i.e., $T_e = 1.36 \times 10^9 \text{ K}$; see Methods) and the equations from eq. (2) to eq. (4) for the optical depth, the photon index, and the IC luminosity, we computed the photon indices of the IC emission and the corresponding X-ray luminosities (i.e., 1–7 keV) with different wind parameters \dot{M}_{-5}/w_{10} (a SN age of 20 days is assumed), which are shown with the best-fit XRT spectral values in Figure 2. Comparing with the *Swift*/XRT data, it is clear that $\dot{M}_{-5}/w_{10} \approx 4$ matches well with the best-fit results. The corresponding optical depth is $\tau_e \approx 0.04$, which fulfils the minimum criterion of $\tau_e > 0.01$. In addition, we also used the UVOT color temperature of the secondary peak (i.e., $T_c \approx 5500 \text{ K}$; see the Methods section) for the same analyses and the result is similar to the previous one with a slightly larger $\dot{M}_{-5}/w_{10} \approx 5$ ($\tau_e \approx 0.05$). Therefore, we conclude that the wind parameter of the progenitor is approximately $\dot{M}_{-5}/w_{10} \approx 4 - 5$.

A free-free emission as the “quiescent” component

We attribute the so-called “quiescent” off-peak X-ray emission component to be a free-free emission of the shocked hot gas as indicated by the extremely flat X-ray spectrum observed (i.e., $\Gamma \approx 1.0$, equivalent to a zero spectral index; See Methods for details). According to Fransson et al.², the free-free luminosity density is also a strong function of \dot{M}_{-5}/w_{10} and a simplified version for $V = 10^4 \text{ km s}^{-1}$ around 1 keV can be written as

$$L_{\text{ff}}(1 \text{ keV}) = 4.9 \times 10^{38} \zeta \left(\frac{\dot{M}_{-5}}{w_{10}} \right)^2 \left(\frac{t}{1 \text{ day}} \right)^{-1} \text{ erg s}^{-1} \text{ keV}^{-1}. \quad (1)$$

By adopting $\zeta = 0.86$ (see Methods) and $\dot{M}_{-5}/w_{10} = 4 - 5$, the free-free X-ray luminosities (i.e., 1–7 keV and $\Delta L_{\text{ff}} = 6 \text{ keV}$) in the time interval of $t = 10 \text{ d}$ to 60 d are in the range of 6×10^{39} to $0.7 \times 10^{39} \text{ erg s}^{-1}$, which are in a good agreement of the *Swift*/XRT data.

Discussion

Chevalier¹³ suggested that such *Compton* scattering radiations should dominate the UV band, equivalent to an energy range around 10–100 eV, while emissions in the X-ray band (i.e. 0.1–10 keV) are mainly caused by free-free scatterings. However, the Comptonization flux could sometimes be compatible to the free-free radiations in soft X-ray band; for instance, the luminosity ratio of the *Compton*-to-free-free processes of SN 1993J (i.e., $L_{\text{Comp}}/L_{\text{ff}}$) in ROSAT range (i.e., 0.1–2.4 keV) for $\tau_e \approx 0.05$ and $T_e \approx 10^9 \text{ K}$ was computed to be 1.36 at day 7² and the ratio could increase to $L_{\text{Comp}}/L_{\text{ff}} = 341$ with an electron temperature of $T_e = 5 \times 10^9 \text{ K}$. Although the ROSAT range is slightly different from the *Swift*/XRT range used here, the electron scattering optical depth as well as the shock temperature are indeed very similar to what

inferred from the *Swift*/XRT peak emission spectrum. This ensures the possibility of the IC scattering scenario in such an optically-thin hot gas. Moreover, the inferred $\dot{M}_{-5}/w_{10} \approx 4 - 5$ of SN 2013df is indeed very close to the one of SN 1993J inferred with the early X-ray data (i.e., $\dot{M}_{-5}/w_{10} \approx 4^2$). While the SN 1993J progenitor has been firmly characterized as an early K-type supergiant star¹⁴, the similarity between the pre-explosion stellar winds of the two SNe suggests that the SN 2013df progenitor was also a yellow supergiant, supporting the cool supergiant detected by the HST⁴ as the true progenitor.

Other Possible Mechanisms

Synchrotron radiation is another possible mechanism to produce non-thermal X-rays in SNe. However, the expected X-ray emission inferred from the observed synchrotron radio spectrum is at least an order of magnitude fainter than what we have seen in SN 2013df⁷. We also considered an inverse *Compton* emission of the synchrotron radio photons as the origin of the observed X-rays, but in this case the X-ray-to-radio ratio would be too large (i.e., the radio luminosity at 5 GHz is $L_R = 2.6 \times 10^{36} \text{ erg s}^{-1}$ and $L_X/L_R > 2000$) comparing with other well-studied SNe (e.g., $L_{\text{IC}}/L_{\text{synch}} < 40$ for the SN 1998bw¹⁵). Therefore, both the above two mechanisms are not applicable in the case of SN 2013df.

Alternatively, it has been suggested that the X-rays of SN 2013df are dominated by the bremsstrahlung thermal emissions from either the forward shock ($T_{\text{fs}} \geq 10^9 \text{ K}$) or the reverse shock ($T_{\text{rs}} \geq 10^7 \text{ K}$)⁷. Although we agree that the free-free emissions significantly contribute the observed X-rays in the early phase (see the previous section), bremsstrahlung alone is insufficient to explain the correlation between the optical/X-ray light curves. While the X-ray photon index of SN 2013df is harder than it should be in a Comptonization dominant case ($\Gamma_{\text{ph}} \approx 3$; see Figure 2), a hybrid of thermal bremsstrahlung and Inverse-*Compton* is a good way to understand the multi-wavelength data as we suggested.

Importance of the Inverse-*Compton* emission for SN studies

Inverse-*Compton* model has been well established to explain X-ray emissions of various SN events, for examples, the Type II-L SNe 1979C, 1980K, the famous Type II-b SN 1993J, and the Type II-P SN 2006bp^{1,2,13,16}. In fact, the IC scenario is also promising to explain the mysterious X-ray emissions of the special class GRB-SN associations (i.e., hydrogen-stripped Type Ic and possibly Ib supernovae detected well after the associated GRBs) and SN shock breakout events^{17–19}. While an IC X-ray brightening has been theoretically shown possible during the optical peaks of the SN^{20,21}, it has been a missing piece before for a long time. Although the recent multi-wavelength study of the Type Ia SN 2011fe (a.k.a., PTF 11kly) in M101 placed a marginal constraint on such a correlation by demonstrating a correlated X-ray/optical light curve profiles²², the X-rays of SN 2011fe are actually undetected (i.e., the X-ray profile was constructed based on three upper-limits) and the corresponding flux upper limits place a 3σ constraint on the progenitor mass loss rate of $\dot{M}_{-5}/w_{10} < 2 \times 10^{-5}$ (note: it could be an interstellar stellar medium instead), which just ambiguously restricts the X-ray/optical relation. The X-ray brightening of SN 2013df shows a clear correlation with the secondary optical peak, which is an important example for the SN ejecta and CSM interaction model.

The IC X-ray component study could also benefit various researches on Type Ia. As stated earlier, Type Ia supernovae are also possible IC X-ray emission sources, although no significant X-ray detection has been made from any known Type Ia (except for the SN 2014J in which ^{56}Co lines at energies of 847 and 1238 keV were detected by INTEGRAL²³). If IC scattering is significant, a few percent (i.e., $\sim \tau_e/2$) of the SN optical radiations will be IC scattered and the optical measurement will deviate from the true intrinsic SN brightness. As Type Ia supernovae are well-known as standard candles to measure cosmological distances by tracing accurately the unique SN decline, the measured brightness deviation could be important to fine-tune the distance ladder. IC emissions are also crucial to distinguish the proposed origins of Type Ia SNe, which are single-degenerate (a main-sequence star or red giant companion) and double-degenerate scenarios (another white dwarf companion), by examining density of the surrounding medium.

On a conservative basis, the connection between the X-ray brightening of SN 2013df and the predicted IC X-ray emission may not be exclusively proven here. Nevertheless, this work certainly provides a new angle to the community on how simultaneous optical/X-ray data can be used to search for the IC emission of SNe. In particular, rapid *Swift* multi-wavelength observations of SNe have been shown to be useful to such a search. Hopefully, *Swift* will bring us more solid evidence of the IC emissions of SNe in the future.

Methods

Swift X-ray Telescope (XRT)

A series of *Swift* ToO observations for SN 2013df was triggered since 2013 June 13 (6 days after the optical discovery) with a total number of 26 observations until 2013 August 6. From the combined 49 ks X-ray Telescope (XRT) observation, a hard X-ray source was detected at $\alpha(\text{J2000}) = 12^{\text{h}}26^{\text{m}}29^{\text{s}}.326$, $\delta(\text{J2000}) = 31^{\circ}13'37''.87$ with an uncertainty of $3.6''$ (radius, 90% confidence), which is less than $0.2''$ offset from the optical position. No significant X-ray source was found at the same position in the previous XMM-*Newton* observations taken in 2005 – 2006 with a 3σ upper limit of $2.96 \times 10^{-15} \text{ erg cm}^{-2} \text{ s}^{-1}$ or $9.8 \times 10^{37} \text{ erg s}^{-1}$ (0.5–4.5 keV) deduced by the XMM-*Newton* FLIX server.

We downloaded the *Swift* observations from the HEASARC archive and extracted XRT spectra and light curves using the HEASOFT (version of 6.11) built-in tasks, `xrtgrb1c` and `xrtgrb1cspec`. The source photons were selected using

a circular region with a radius of $15''$ while a background subtraction was done using a source-free annulus region around the host galaxy. Unless otherwise mentioned, the uncertainties are in 90% confidence level.

The *Swift*/XRT light curve (Figure 1; at least 10 counts per bin with *Poisson* errors) shows that the X-ray emission lasted for about fifty-five days since the first *Swift* observation, during which the X-rays gradually rises from $\sim 5 \times 10^{39} \text{ erg s}^{-1}$ at day 7 (with respect to the SN discovery here), reaches a peak luminosity of $\sim 1 \times 10^{40} \text{ erg s}^{-1}$ at about day 18, and drops steadily over the last 40 days of observations (Figure 1). For the spectral model fitting, the XRT spectrum was binned with at least 15 counts per bin and weighted with the *Gehrels* approximation²⁴ (i.e., $\sigma \approx 1 + \sqrt{N+0.75}$ for a bin with N counts) for a better uncertainty estimation in cases of $N < 20$. We fitted the averaged “hard” XRT spectrum (i.e., 1–7 keV; to avoid possible contaminations from the soft X-ray diffuse emission of the host galaxy) with an absorbed power law model, of which the best-fit values are $N_{\text{H}} < 2.6 \times 10^{22} \text{ cm}^{-2}$ and $\Gamma_{\text{ph}} = 0.91_{-0.6}^{+1.4}$ ($\chi^2_{\text{v}} = 0.82$ with $dof = 3$). In addition, we tried a thermal bremsstrahlung model to fit the data, but the best-fit plasma temperature hit the boundary (i.e., 200 keV) to fail the fit. Thus, we fixed the temperature to $kT = 100 \text{ keV}$ (or $T_e \sim 10^9 \text{ K}$, a typical temperature of a free-free X-ray emission for supernovae²), which cured the fit and gave $N_{\text{H}} < 1.6 \times 10^{22} \text{ cm}^{-2}$ and $\chi^2_{\text{v}} = 0.66$ ($dof = 4$). Though a smaller χ^2_{v} value than that of the power-law model was obtained, we do not consider the improvement significant as the χ^2_{v} becomes 0.62 ($dof = 4$) if we fixed the photon index to $\Gamma_{\text{ph}} = 1$. Instead, the simple power-law and the thermal bremsstrahlung models are both significant to describe the data and the former model fits the spectrum slightly better.

As the photoelectric absorption is much more important below 1 keV, we extended the lower energy range of the XRT spectrum down to 0.3 keV to have a better constraint on the column density, hence to improve the fits. We also set the minimum allowed column density to the Galactic value²⁵ of $N_{\text{H}} = 1.6 \times 10^{20} \text{ cm}^{-2}$ to prevent a non-logical null absorption. For an absorbed power law, the best-fit parameters are improved to $\Gamma_{\text{ph}} = 0.96_{-0.36}^{+0.50}$ and $N_{\text{H}} < 2.4 \times 10^{21} \text{ cm}^{-2}$ ($\chi^2_{\text{v}} = 0.78$ with $dof = 5$; Figure 3) yielding an unabsorbed luminosity of $L_{0.3-7\text{keV}} \approx 6.8 \times 10^{39} \text{ erg s}^{-1}$. For an absorbed thermal bremsstrahlung (temperature fixed to 100 keV), the best-fit N_{H} changes to $N_{\text{H}} < 2.9 \times 10^{21} \text{ cm}^{-2}$ ($\chi^2_{\text{v}} = 0.84$ with $dof = 6$) and the luminosity is $L_{0.3-7\text{keV}} \approx 6.5 \times 10^{39} \text{ erg s}^{-1}$. Considering the poorly constrained N_{H} , we also computed the “hard” X-ray luminosity $L_{1-7\text{keV}} \approx 6.1 \times 10^{39} \text{ erg s}^{-1}$ (power-law) and $L_{1-7\text{keV}} \approx 5.5 \times 10^{39} \text{ erg s}^{-1}$ (bremsstrahlung), with which the influence of the greatly uncertain N_{H} on the investigation can be minimized.

The X-ray brightening

As mentioned earlier, an X-ray brightening is seen between day 12 and 25. We found that the brightening light curve can be described by a *Gaussian* function on top of a flat light curve, $A \times \exp(-(t-t_p)^2/(2\sigma^2)) + B$, where the best-fit values are $A = (4.8 \pm 0.8) \times 10^{-3} \text{ cts s}^{-1}$, $t_p = 17.1 \pm 0.7 \text{ d}$ (time at the peak), $\sigma = 5.3 \pm 0.8 \text{ d}$, and $B = (2.0 \pm 0.2) \times 10^{-3} \text{ cts s}^{-1}$ ($\chi^2 = 1.6$; $dof = 5$). Alternatively, one may consider the apparent brightening as a statistical fluctuation. In this case, we have modelled the data with a flat light curve and the best-fit count rate is $(2.9 \pm 0.5) \times 10^{-3} \text{ cts s}^{-1}$ ($\chi^2 = 18.6$; $dof = 8$). Clearly, there is a significant improvement (i.e., $\Delta\chi^2 = 17$) when considering the brightening a real detection (i.e., the *Gaussian* model) rather than a fluctuation (i.e., the flat model). To find out whether this improvement is significant, we performed *Monte Carlo* simulations by generating 10^6 flat light curves and fitting them with both models. Among the 10^6 trials, 141208 of them did not converge in the *Gaussian* fit (i.e., a *Gaussian* is totally unnecessary in these cases), 858765 of them have an improvement less than $\Delta\chi^2 = 17$, and only 27 trials were improved by $\Delta\chi^2 \geq 17$. This clearly shows that the X-ray brightening detection is not likely produced by chance (i.e., p -value $\approx 0.003\%$ or statistical significance $\sim 4\sigma$).

To investigate spectral features of the X-ray brightening, we used the observations of IDs from 32862008 to 32862015 to extract a stacked X-ray peak spectrum. Given that the photon statistic is not good (i.e., spectral source counts: 28), we adopted a binning factor of at least 7 counts per bin to produce a 4-bin X-ray spectrum. To elaborate the small binning factor applied, it is a strategy that sacrifices the signal-to-noise (S/N) ratios of single bins to exchange for a larger number of degree-of-freedom. Otherwise, there will be only 1 or 2 bin(s) in the spectrum and leave no freedom for fitting. In fact, low-count binning is common in X-ray astronomy for faint sources (e.g., the *Chandra* spectral analysis of A0620-00²⁶). Additionally, we applied the *W-statistic* (*CASH-statistic*²⁷ with *Poisson* distributed background) to deal with the fitting process, instead of the standard *Chi-squared statistic* (i.e., *Gaussian* distribution is assumed), which does not work properly for low-count spectra (see the [XSPEC on-line manual](#) for details; the difference between *W-statistic* and *Chi-squared* performances is shown in Figure 2). This *W-statistic* (or *CASH-statistic*) has been widely used in spectral fitting with low-count X-ray spectra (e.g., the hyperluminous X-ray source candidate, CXO J122518.6+144545^{28,29}). It is therefore a valid statistical model for the cases of SN 2013df. Although our data have a low number of photon counts, the quality of the spectral fits can be reflected by the uncertainties of the estimated parameters given a proper statistic applied. We also note that spectral binning is not a necessary process for *W-statistic* fitting. However, binned spectra provide χ^2 values of the best fits (not the fitting statistic though) that are good indicators of the goodness-of-fit (i.e., one cannot tell the goodness-of-fit from the *W-statistic*) to guide our data analysis.

With the Galactic hydrogen column density of $N_{\text{H}} = 1.6 \times 10^{20} \text{ cm}^{-2}$ assumed, the spectrum could be power-law distributed with a photon index of $\Gamma_{\text{ph}} = 1.4 \pm 0.6$ and the averaged luminosity of the X-ray peak is $L_{0.3-7\text{keV}} \approx 8.1 \times 10^{39} \text{ erg s}^{-1}$ (or $L_{1-7\text{keV}} \approx 6.6 \times 10^{39} \text{ erg s}^{-1}$). Comparing with the “quiescent” spectrum extracted from the off-peak observations (i.e., Ob. ID: 32862001–00032862005, 32862016–00032862027; Table 1), of which the best-fit values are $\Gamma_{\text{ph}} = 1.0 \pm 0.4$ and $L_{0.3-7\text{keV}} \approx 4.9 \times 10^{39} \text{ erg s}^{-1}$ (or $L_{1-7\text{keV}} \approx 4.4 \times 10^{39} \text{ erg s}^{-1}$), the peak X-ray emissions are spectrally softer, although insignificant. We also tried to subtract the peak spectrum by the “quiescent” one to probe for any additional emission component (i.e. IC emissions) leading to the X-ray enhancement as the observed peak. Two

approaches have been used to eliminate the “quiescent” emission contribution, either by the observed spectrum itself (i.e., serving the “quiescent” spectrum as the “background” spectrum; namely approach *A*) or the best-fit power law model (i.e., including the fixed best-fit “quiescent” spectral model of $\Gamma_{\text{ph,fix}} = 1.0$ and $\text{norm}_{\text{fix}} = 1.4 \times 10^{-5}$ photons $\text{keV}^{-1} \text{cm}^{-1} \text{s}^{-1}$ at 1 keV, to the model of interest; approach *B*). For the approach *A*, the subtracted spectrum can be described with a photon index of $\Gamma = 1.7^{+1.2}_{-1.0}$ and an X-ray luminosity of $L_{0.3-7\text{keV}} \approx 4.3 \times 10^{39} \text{ erg s}^{-1}$ (or $L_{1-7\text{keV}} \approx 3.2 \times 10^{39} \text{ erg s}^{-1}$). For the approach *B* (i.e., two power-law components of which the “quiescent” one has been entirely frozen), the best-fit photon index and X-ray luminosity are $\Gamma = 1.7^{+1.5}_{-1.2}$ and $L_{0.3-7\text{keV}} \approx 3.6 \times 10^{39} \text{ erg s}^{-1}$ (or $L_{1-7\text{keV}} \approx 2.5 \times 10^{39} \text{ erg s}^{-1}$), respectively. While the fitting results of both methods are consistent with each other, the approach *A* generally performs better than the approach *B* in terms of the uncertainties of the best-fit parameters. Figure 2 shows the contour maps of the best-fit photon indices and luminosities, which fully revealed their uncertainties. Combining with the IC emission spectral model for SNe, the maps are indeed very useful to constrain the wind parameter of the SN progenitor (i.e., $\dot{M}_{-5}/w_{10} \approx 4-5$ for a shock velocity of $V_s = 10^4 \text{ km s}^{-1}$).

Swift Ultraviolet and Optical Telescope (UVOT)

Swift/UVOT observed SN 2013df simultaneously with XRT using all six UVOT filters (central wavelengths are from 1928 to 5468 Å). We used a HEASOFT task `uvotmaghist` to compute the magnitude/flux density of each UVOT image using an aperture radius of $3''$ (the optimum aperture size for UVOT images; see the [Swift/UVOT on-line analysis thread](#) for details) with an annulus source-free background around the SN. A prominent double-peaked light curve feature of Type IIb is clearly shown in v and b bands, but marginally seen from u to $um2$ bands and invisible in $uw2$ band (Figure 1). The extinction corrected UVOT magnitudes of the first and second peaks are listed in Table 2 with $A_v = 0.30 \text{ mag}$ ¹¹. Based on the relation between $B-V$ colors and color temperatures (T_c in Kelvin) for blackbody radiations (i.e., $B-V \approx (7090/T_c) - 0.71$), inferred temperatures of the peaks are $T_c = 8500 \pm 4000 \text{ K}$ and $T_c = 5500 \pm 800 \text{ K}$ for the first and second peaks, respectively. These temperatures are roughly consistent with those obtained by optical spectroscopic fittings in Morales-Garoffolo et al.¹¹ (i.e., $T_c = 7700 \pm 500 \text{ K}$ at day 9 and $T_c = 6900 \pm 500 \text{ K}$ at day 22).

The IC emission spectral model for SNe

According to Fransson et al.², the electron scattering optical depth behind the circumstellar shock is dependent of the shock velocity (V_s) and the stellar wind properties, which could be described as (note: it is a modified version for general uses as the original version is dedicated for the Type IIb SN 1993J, see Fransson et al. 1996² and references therein for details):

$$\tau_e = 2.314 \times 10^{-1} \zeta \left(\frac{\dot{M}_{-5}}{w_{10}} \right) \left(\frac{V_s}{10^4 \text{ km s}^{-1}} \right)^{-1} \left(\frac{t}{1 \text{ day}} \right)^{-1}. \quad (2)$$

The \dot{M}_{-5}/w_{10} is the key parameter for the stellar wind description, where \dot{M}_{-5} is the mass-loss rate in units of $10^{-5} M_{\odot} \text{ yr}^{-1}$ and w_{10} is the wind velocity in units of 10 km s^{-1} . There is another parameter ζ , defined as $\zeta = (1 + 2n_{\text{He}}/n_{\text{H}})/(1 + 4n_{\text{He}}/n_{\text{H}})$ for describing the chemical composition of the wind and $n_{\text{He}}/n_{\text{H}} = 0.1$ is assumed throughout this analysis (i.e., $\zeta = 0.86$, which has been widely used to explain the X-ray emission of SN 1993J²). In addition, the formula is constructed under an assumption of a steady stellar wind flow (i.e., $\rho_w \propto r^{-2}$), which is the simplest case of a circumstellar density profile. Fransson¹ has shown that there is a fraction of $\sim (\tau_e/2)^n$ of the supernova photospheric blackbody radiation up-scattered n times by the energetic shock electrons to form high-energy X-ray emissions, even though the hot shock gas is optical thin to electron scattering. For optical depths smaller than $\tau_e \ll 0.01$, each seed photon will at most be up-scattered only one time before it escapes the hot shock. In this case, the energies of the IC scattered photons will be doubled (i.e., $\Delta E/E \approx 4kT_s/m_e c^2 \approx 1$ for $4kT_s \gg E$, with a typical shock temperature $T_s \approx 10^9 \text{ K}$) to possibly produce an excess UV tail at the shorter wavelength end of the blackbody spectrum, but certainly no X-rays in keV levels. For $\tau_e > 0.01$, the number of electron scattering is large (i.e., $n > 1$) and the Compton cooling is therefore important. In this case, the Comptonized spectrum is a single power-law in X-rays (i.e., $N(E) \propto E^{-\gamma}$), with a photon index of

$$\gamma = (9/4 - \ln((0.9228 - \ln(\tau_e))\tau_e/2)/\alpha)^{1/2} - 1/2, \quad (3)$$

where $\alpha = kT_s/m_e c^2$ (note: the γ index is a spectral index (i.e., $F(E) \propto E^{-\gamma}$), instead of a photon index, in the original version¹). The Compton luminosity above 13.6 eV could be described by a semi-empirical expression as

$$L_{\text{Comp}} = 4.5 \times 10^{40} \left(\frac{R_p}{10^{15} \text{ cm}} \right) \left(\frac{\tau_e}{0.01} \right) \left(\frac{T_{\text{eff}}}{10^4} \right)^{\gamma+2} \left(\frac{T_s}{10^9 \text{ K}} \right) \text{ erg s}^{-1}, \quad (4)$$

where R_p and T_{eff} are the radius and the temperature of the photosphere, respectively, and T_s is the temperature of the shocked gas. According to Fransson et al.¹², the shock temperature can be computed for a given shock velocity V_s by

$$T_s = 1.36 \times 10^9 \left(\frac{V_s}{10^4 \text{ km s}^{-1}} \right) \text{ K.} \quad (5)$$

The inferred shock temperature (T_s) is also the temperature of ions (T_{ion}) in the shocked hot gas. As the equipartition time of the plasma is relatively short (i.e., about 1 day) in such a high density shocked region, the ion temperature is approximately the same as the electron temperature (i.e., $T_e \approx T_{\text{ion}}$)¹.

References

1. Fransson, C. X-ray and UV-emission from supernova shock waves in stellar winds. *Astron. & Astrophys.* **111**, 140–150 (1982).
2. Fransson, C., Lundqvist, P. & Chevalier, R. A. Circumstellar Interaction in SN 1993J. *Astrophys. J.* **461**, 993 (1996).
3. Ciabattari, F. *et al.* Supernova 2013df in NGC 4414 = Psn J12262933+3113383. *CBETs* **3557**, 1 (2013).
4. Van Dyk, S. D. *et al.* The Type IIb Supernova 2013df and its Cool Supergiant Progenitor. *Astron. J.* **147**, 37 (2014).
5. Li, K. L. & Kong, A. K. H. X-ray detection of SN 2013df. *ATel* **5150**, 1 (2013).
6. Perez-Torres, M. *et al.* eMERLIN radio detection of SN2013df at 5.0 GHz. *ATel* **8452**, 1 (2015).
7. Kamble, A. *et al.* Radio and X-rays From SN 2013df Enlighten Progenitors of Type IIb Supernovae. *ArXiv e-prints (submitted to Astrophys. J.)* **arXiv:1504.07988**, 1–15 (2015).
8. Freedman, W. L. *et al.* Final Results from the Hubble Space Telescope Key Project to Measure the Hubble Constant. *Astrophys. J.* **553**, 47–72 (2001).
9. Claeys, J. S. W., de Mink, S. E., Pols, O. R., Eldridge, J. J. & Baes, M. Binary progenitor models of type IIb supernovae. *Astron. & Astrophys.* **528**, A131 (2011).
10. Woosley, S. E., Eastman, R. G., Weaver, T. A. & Pinto, P. A. SN 1993J: A Type IIb supernova. *Astrophys. J.* **429**, 300–318 (1994).
11. Morales-Garoffolo, A. *et al.* SN 2013df, a double-peaked IIb supernova from a compact progenitor and an extended H envelope. *Mon. Not. R. astr. Soc.* **445**, 1647–1662 (2014).
12. Fransson, C. Comptonization and UV emission lines from Type II supernovae. *Astron. & Astrophys.* **133**, 264–284 (1984).
13. Chevalier, R. A. The radio and X-ray emission from type II supernovae. *Astrophys. J.* **259**, 302–310 (1982).
14. Van Dyk, S. D. *et al.* The Progenitor of Supernova 1993J Revisited. *PASP* **114**, 1322–1332 (2002).
15. Kulkarni, S. R. *et al.* Radio emission from the unusual supernova 1998bw and its association with the γ -ray burst of 25 April 1998. *Nature* **395**, 663–669 (1998).
16. Immler, S. *et al.* X-Ray, UV, and Optical Observations of Supernova 2006bp with Swift: Detection of Early X-Ray Emission. *Astrophys. J.* **664**, 435–442 (2007).
17. Soderberg, A. M. *et al.* An extremely luminous X-ray outburst at the birth of a supernova. *Nature* **453**, 469–474 (2008).
18. Waxman, E., Mészáros, P. & Campana, S. GRB 060218: A Relativistic Supernova Shock Breakout. *Astrophys. J.* **667**, 351–357 (2007).
19. Hjorth, J. & Bloom, J. S. *The Gamma-Ray Burst - Supernova Connection*, 169–190 (Cambridge University Press (Cambridge), 2012).
20. Björnsson, C.-I. & Fransson, C. The X-Ray and Radio Emission from SN 2002ap: The Importance of Compton Scattering. *Astrophys. J.* **605**, 823–829 (2004).
21. Chevalier, R. A. & Fransson, C. Circumstellar Emission from Type Ib and Ic Supernovae. *Astrophys. J.* **651**, 381–391 (2006).
22. Margutti, R. *et al.* Inverse Compton X-Ray Emission from Supernovae with Compact Progenitors: Application to SN2011fe. *Astrophys. J.* **751**, 134 (2012).
23. Churazov, E. *et al.* Cobalt-56 γ -ray emission lines from the type Ia supernova 2014J. *Nature* **512**, 406–408 (2014).
24. Gehrels, N. Confidence limits for small numbers of events in astrophysical data. *Astrophys. J.* **303**, 336–346 (1986).
25. Kalberla, P. M. W. *et al.* The Leiden/Argentine/Bonn (LAB) Survey of Galactic HI. Final data release of the combined LDS and IAR surveys with improved stray-radiation corrections. *Astron. & Astrophys.* **440**, 775–782 (2005).
26. Kong, A. K. H., McClintock, J. E., Garcia, M. R., Murray, S. S. & Barret, D. The X-Ray Spectra of Black Hole X-Ray Novae in Quiescence as Measured by Chandra. *Astrophys. J.* **570**, 277–286 (2002).

27. Cash, W. Parameter estimation in astronomy through application of the likelihood ratio. *Astrophys. J.* **228**, 939–947 (1979).
28. Jonker, P. G. *et al.* A bright off-nuclear X-ray source: a type II_n supernova, a bright ULX or a recoiling supermassive black hole in CXOJ122518.6+144545. *Mon. Not. R. astr. Soc.* **407**, 645–650 (2010).
29. Heida, M., Jonker, P. G. & Torres, M. A. P. Discovery of a second outbursting hyperluminous X-ray source. *Mon. Not. R. astr. Soc.* **454**, L26–L30 (2015).

Acknowledgements

This project was supported by the Ministry of Science and Technology of Taiwan through grant 103-2628-M-007-003-MY3. Special thanks are given to Thomas P. H. Tam, Hsiang-Kuang Chang, Tomotsugu Goto, and Yi Chou for helpful discussions.

Author contributions statement

Data analysis: KLL; data interpretation: KLL and AKHK; manuscript: KLL and AKHK.

Additional information

The author(s) declare no competing financial interests.

Table 1. *Swift*/XRT Observation log of SN 2013df

Date	Ob. ID	Exposure Time (s)	Note
5.94	32862001	2969.27	Low
8.36	32862002	1977.85	Low
9.95	32862003	139.86	Low
8.68	32862005	1940.39	Low
10.62	32862006	3348.88	Raising
10.62	32862007	489.50	Raising
11.69	32862008	497.00	Peak
11.69	32862009	2677.11	Peak
12.70	32862010	2310.00	Peak
15.23	32862011	1578.28	Peak
16.84	32862012	1523.35	Peak
18.57	32862013	1800.55	Peak
23.30	32862014	2170.14	Peak
24.92	32862015	1947.89	Peak
27.17	32862016	1573.29	Low
28.78	32862017	1997.83	Low
30.78	32862018	1840.50	Low
33.26	32862019	1353.55	Low
35.25	32862020	1221.18	Low
36.65	32862021	1558.31	Low
38.80	32862022	1156.25	Low
45.66	32862023	3638.54	Low
49.93	32862024	1086.33	Low
53.61	32862025	4060.58	Low
58.48	32862026	452.01	Low
59.62	32862027	3940.71	Low

Table 2. *Swift*/UVOT magnitudes of SN 2013df

	<i>v</i>	<i>b</i>	<i>u</i>	<i>uvw1</i>	<i>uvm2</i>	<i>uvw2</i>
1st Peak	14.47 (0.04)	14.59 (0.04)	13.67 (0.05)	14.09 (0.05)	14.31 (0.05)	14.77 (0.06)
2nd Peak	14.30 (0.06)	14.87 (0.06)	14.67 (0.07)	15.17 (0.06)	15.58 (0.07)	...

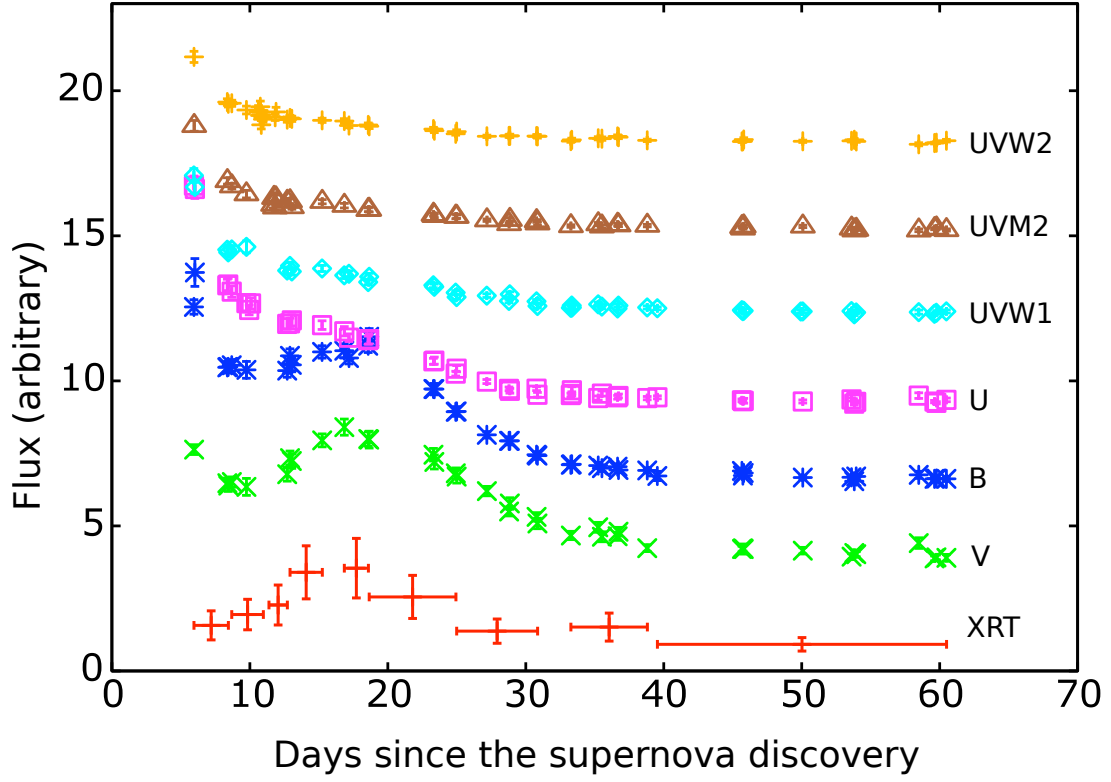


Figure 1. Multi-wavelength light curves of SN 2013df with day zero fixed at the SN discovery.

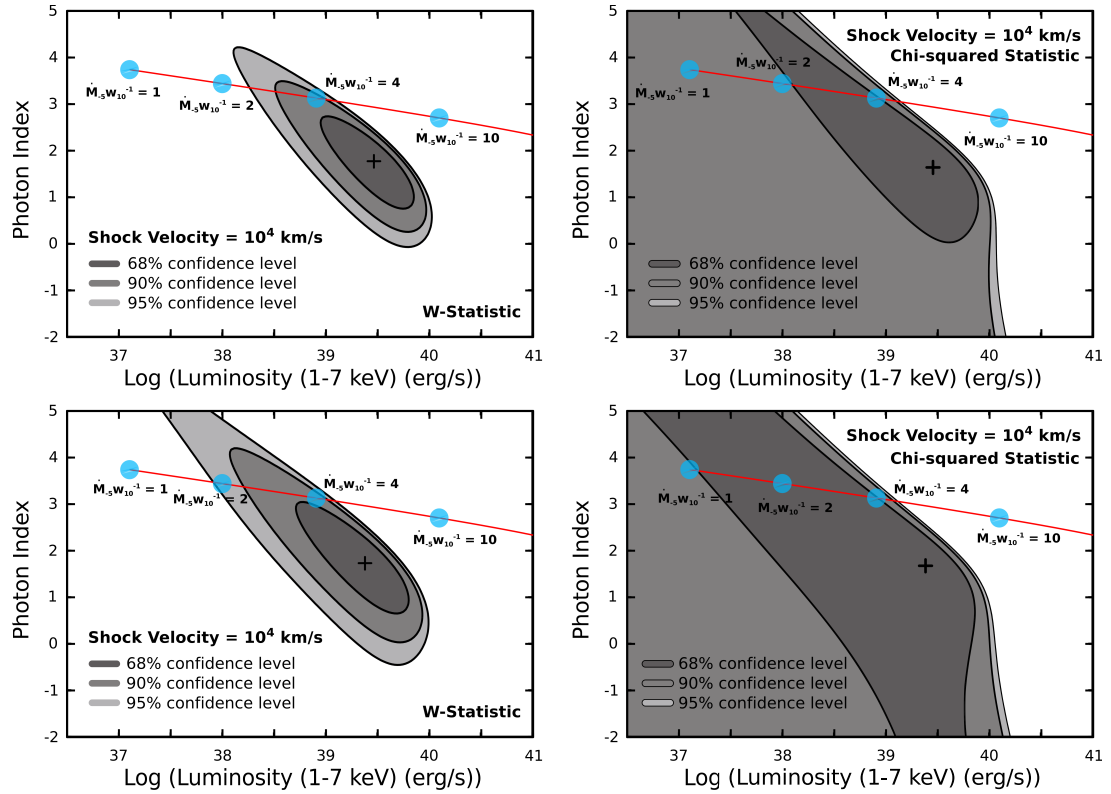


Figure 2. Photon index versus logarithmic scale luminosity of the SN Comptonization model (red line; a SN photosphere of $T_c = 6900$ K is assumed) plotted with contours of the best-fit at 68%, 90%, and 95% confidence levels (grey shadows). The upper two plots are based on Approach A while the lower two are based on Approach B (see the text for details).

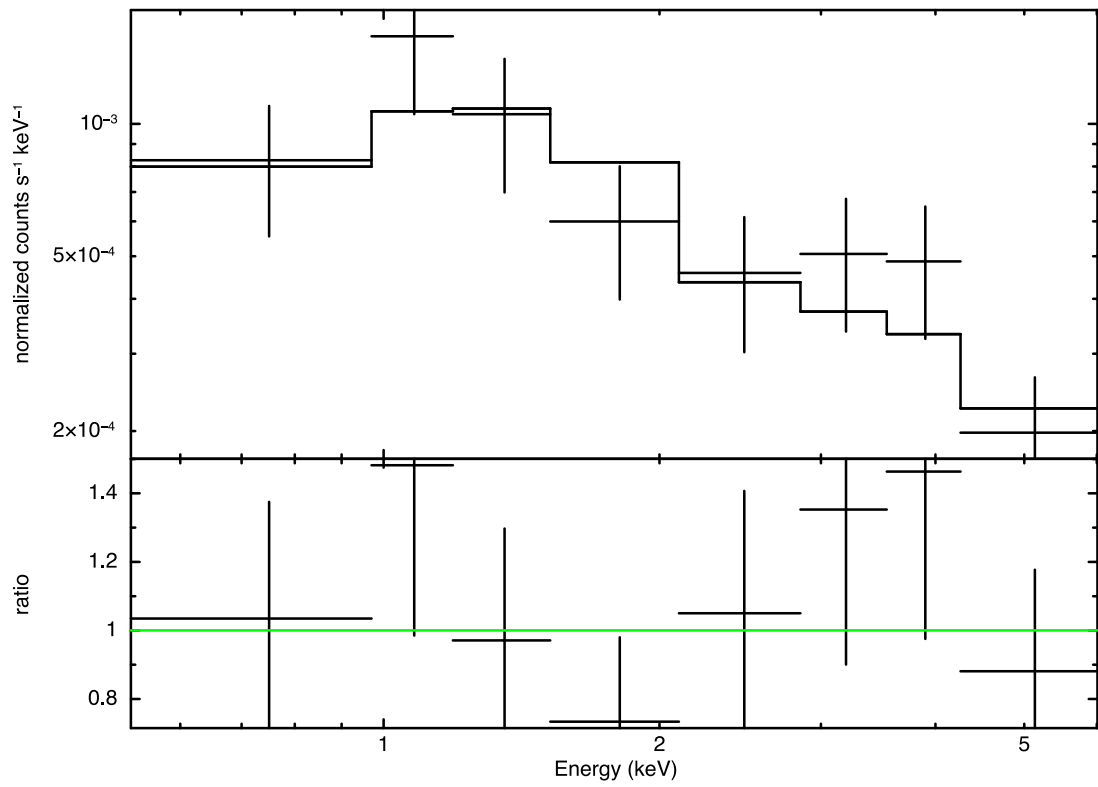


Figure 3. *Swift*/XRT spectrum of SN 2013df with the best-fit power-law of $\Gamma_{\text{ph}} = 0.96^{+0.50}_{-0.36}$ and $N_{\text{H}} < 2.4 \times 10^{21} \text{ cm}^{-2}$ ($\chi^2_{\nu} = 0.78$ with $dof = 5$).